1 Measurements of stellar magnetic fields

The astronomer G. E. Hale is well known for his pioneering work on the magnetic field of sunspots. Combining state-of-the-art measurement techniques with the latest advances in physics, he was the first to realize that the splitting (or broadening) in solar absorption lines across sunspots is attributable to the magnetically induced Zeeman effect (see Fig. 1).

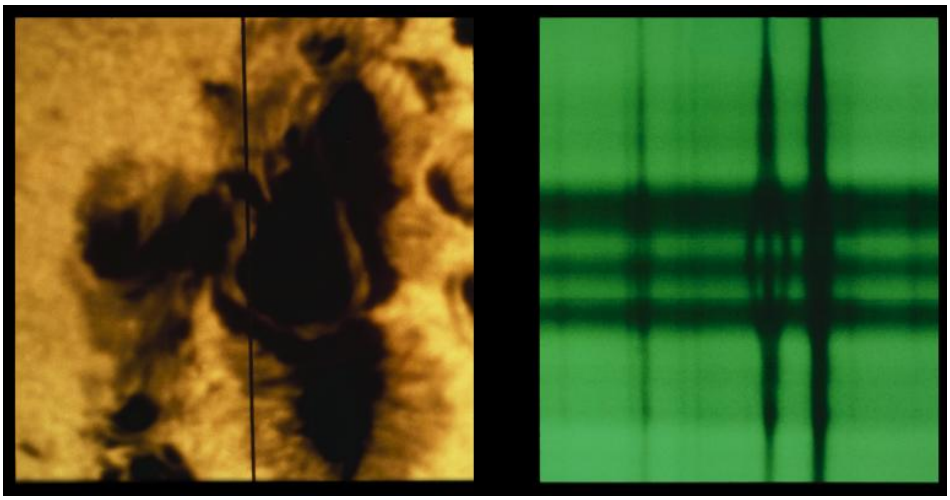

Figure 1: Magnetically induced line splitting in sunspot region. Left: Optical sunspot image with spectrograph slit indicated as a vertical line. Right: Position-dependent spectrum (wavelength on abscissa and position on ordinate).

His work and, in particular, his 1908 paper, cautiously entitled "On the Probable Existence of a Magnetic Field in Sun-Spots" (Hale 1908), laid the foundation for our understanding of the solar and stellar magnetic field and, more generally, stellar activity. A concise review of his achievements is given by Harvey (1999).

1.1 The Zeeman effect

The Hamilton operator of an isolated atom in a magnetic field with central potential and spin-orbit-coupling (in Gaussian units) is given by

$$H = -\frac{\hbar^2}{2cm}\nabla^2 + V(r) + \xi(r)\vec{L}\cdot\vec{S} + \left[-\frac{e}{2mc}\vec{B}\cdot(\vec{L}+2\vec{S}) + \frac{e^2}{8mc^2}B^2r^2\sin^2(\theta)\right] , \qquad (1)$$

where m is the electron mass, e the elementary charge, c the speed of light, $\vec{L}$ is the orbital angular momentum, and $\vec{S}$ the spin. The function ξ is given by

$$\xi(r) = \frac{\mu_B}{\hbar mec^2}\frac{1}{r}\frac{\partial V}{\partial r} \quad \text{with} \quad \mu_B = \frac{\hbar}{2mc} \quad \text{and (here)} \quad V \sim \frac{1}{r} . \qquad (2)$$

In Eq. 1, the two summands in brackets describe the effect of the magnetic field. The second summand is also called the "diamagnetic term".

According to the relative importance of the individual terms, the magnetic field causes different effects. These are the linear and quadratic Zeeman effect and the Paschen-Back effect. The respective requirements are detailed in Table 1, where the spin-orbit term is abbreviated as H_{LS}, the linear magnetic term as H_B, and the quadratic (diamagnetic) term as H_{B^2}.
An idea of the relevant field strengths can be obtained by substituting $L \approx \hbar$, $r \approx a_0$, and $V \approx e/a_0$, where a_0 is the Bohr radius. The calculation yields that

1. for $B < 50$ kG the linear Zeeman effect dominates,

Table 1: The magnetic regimes and effects caused by the magnetic field.

Condition(s)	Effect
$H_{B^2} << H_B << H_{LS}$	Linear Zeeman effect
$H_{B^2} << H_B$ & $H_{LS} << H_B$	Paschen-Back effect
$H_{B^2} >> H_B$ & $H_{B^2} >> H_{LS}$	Quadratic Zeeman effect

2. for $B > 100$ kG the quadratic term starts to become important,

3. for $B < 10^{7-8}$ G the magnetic terms remain small compared to the Coulomb term.

The latter condition is crucial to allow the application of perturbation theory. Beyond this limit, calculations become dramatically more complicated. While the above field strengths provide orientation, the exact conditions depend on the actual atomic configuration.

1.2 The linear Zeeman effect

For low magnetic field strengths, the atom is only weakly disturbed by the linear magnetic term (see Eq. 1). In this case, the energy level is split into $2J + 1$ sublevels, where J is the total angular momentum. The energies of the sublevels are given by

$$E_i = E_{i,0} + g_i \left(\frac{e}{2mc}\right) B m_J \hbar \quad \text{with} \quad m_J = -J, -J+1 \ldots, J \; . \tag{3}$$

Here, m_J is the magnetic quantum number and g_i is the Landé factor. Assuming spin-orbit-coupling (LS-coupling), the Landé factor can be calculated by

$$g_i = 1 + \left(\frac{J(J+1) + S(S+1) - L(L+1)}{2J(J+1)}\right) \; . \tag{4}$$

However, experimental results can substantially deviate (Mathys 1989, Sect. 2.2.3). For specific combinations of the quantum numbers, Landè factors of zero can be produced (Eq. 4). The resulting lines show no magnetic splitting and are called "null lines". Such null lines represent an important reference in the measurement of magnetic fields.
The energy splitting leads to closely spaced transitions with frequencies

$$\nu_{i,j} = \frac{E_i - E_j}{h} = \nu_0 + \left(\frac{e\hbar B}{2mch}\right) (g_i m_i - g_j m_j) \; . \tag{5}$$

Allowed transitions occur for $m_j = m_i + (-1, 0, +1)$. Spectral lines pertaining to transitions with $\Delta m = m_j - m_i = \pm 1$ are called "σ-components" and transitions without change in the magnetic quantum number are called "π-components". The σ-components are further subdivided into σ_+-components for which $\Delta m = +1$ and, analogously, σ_--components. An example of allowed transitions is given in Fig. 2. The associated wavelengths are given by

$$\lambda_{ij} = \lambda_0 + \left(\frac{e\lambda_0^2 B}{4\pi mc^2}\right) (g_j m_j - g_i m_i) = \lambda_0 + \left(\frac{e\lambda_0^2 B}{4\pi mc^2}\right) [(g_j - g_i) m_j + g_i \Delta m] \; . \tag{6}$$

The expression can partially be evaluated to yield

$$\lambda_{ij} = \lambda_0 + 4.67 \times 10^{-13} \text{ Å}^{-2} \, \text{G}^{-1} \, \lambda_0^2 B (g_j m_j - g_i m_i) \; . \tag{7}$$

For a spectral line at a wavelength of 5000 Å and a magnetic field of 1 kG, the resulting separation between π and σ components, $\Delta\lambda$, is 0.012 Å. Note that the splitting is proportional to the square of the line wavelength, λ_0, which favors observations at larger wavelengths.

If the Landé factors g_j and g_i are equal or (at least) one of the levels participating in the transition shows no split (i.e., $J = 0$ or $g = 0$), the π and σ components merge. Unless in such a case *all* transitions occur at the same wavelength, the so-called Zeeman-triplet is produced. This is usually dubbed the "normal Zeeman effect". Generally, however, the Landé factors are different and more line components are produced. For historical reasons, this is called the "anomalous Zeeman effect".

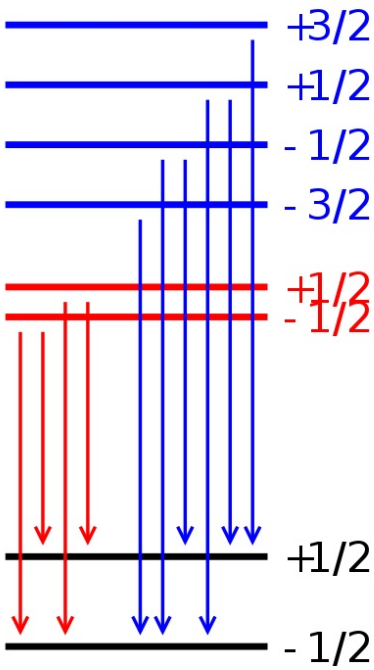

Figure 2: Demonstration of the magnetic splitting of energy levels and allowed transitions. The blue arrows show allowed transitions from a $J = 3/2$ to a $J = 1/2$ level and the red arrow indicate allowed transition from between two $J = 1/2$ levels. Generally, σ-components pertain to $\Delta m = \pm 1$ transitions and π-components to $\Delta m = 0$ transitions (Credit: Evgeny `https://commons.wikimedia.org/wiki/File:Zeeman_p_s_doublet.svg`).

1.3 The Paschen-Back effect

In this regime, the magnetic field is strong enough to break the coupling of orbital angular momentum (L) and spin (S). The energy of the resulting sublevels becomes

$$E_i = E_{i,0} + \left(\frac{e\hbar}{2mc}\right) B(m_L + 2m_S) \; . \tag{8}$$

Allowed transitions occur for $\Delta m_L = 0, \pm 1$ and $\Delta m_S = 0$, so that a triplet is produced. Note that the width of the energy split does not show a dependence on wavelength for the Paschen-Back effect.

1.4 Appearance of the Zeeman triplet

Figure 3 shows the appearance of the Zeeman triplet with a central π-component and two flanking σ-components. Note that the appearance of the Zeeman triplet is intimately related to the orientation of the magnetic field to the observer's line of sight. While all components are present in the case of a transverse field, the π-component(s) vanish(es) when the magnetic field is longitudinal, i.e., parallel to the line of sight.

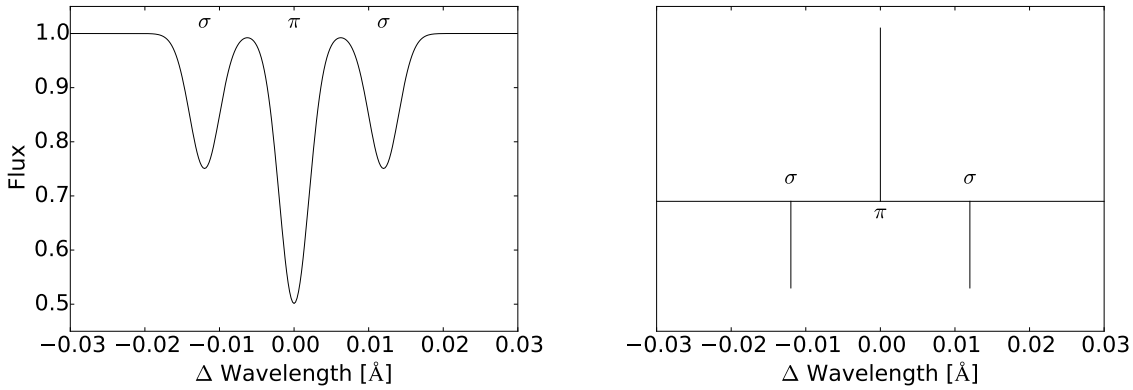

Figure 3: Appearance of the Zeeman triplet. Left: Sketch of a Zeeman triplet spectrum. The central π-component is flanked by two σ-components appearing on either side of the central component. Right: Commonly used representation of the Zeeman pattern with π-components above the horizontal line and σ-components below. The length of the individual lines encodes the associated line strength.

In general, the Zeeman pattern is more complex than the triplet depicted in Fig. 3 with more individual components. A common characteristics of all Zeeman patterns is their symmetry around the central wavelength (Mathys 1989).

1.5 Magnetic field measurements in Ap stars

Ap-stars are chemically peculiar A-type stars (i.e., $T_{\rm eff} \approx 8000$ K) showing unusual abundances, e.g., of chromium, manganese, silicon, and rare earth elements (scandium, yttrium, etc.). About 10 % of the upper main-sequence stars show such peculiar abundances (e.g., Landstreet 1992). Moreover, these elements are inhomogeneously distributed across the stellar surface.

1.5.1 The mean magnetic field modulus

Using the splitting of the Fe II line at 6149.2 Å, the mean magnetic field modulus, i.e., the intensity-weighted magnetic field across the visible stellar hemisphere, can be measured (Mathys et al. 1997). The λ6149.2 Å line results from a transition between two $J = 1/2$ levels (see Fig. 4). Of the participating levels, one shows strong magnetic splitting with a Landè factor of 2.7, while the other level has a Landè factor of zero and shows no splitting (the splitting indicated in Fig. 4 is only for clarity).

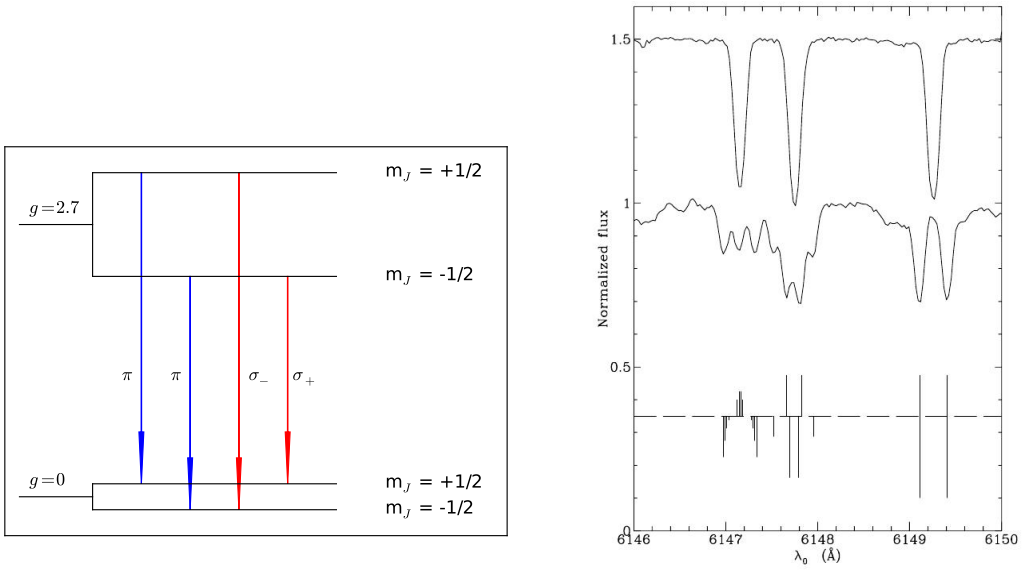

Figure 4: The Fe II λ6149.2 Å line. Left: The formation of the Zeeman components of the Fe II λ6149.2 Å transition. Right: Observed magnetic splitting in HD 94660 (middle) and reference spectrum of HD 133792 (top). The Zeeman pattern is illustrated by the bottom line (figure from Mathys et al. 1997, their Fig. 1).

The λ6149.2 Å line shows two π- and two σ-components. As a result of the absence of magnetic splitting in one level, the π- and σ-components resulting from the same sublevel of the split energy state merge. Therefore, both transverse and longitudinal field orientations give rise to the same splitting of the spectral line. An example of the resulting spectrum is shown in the right panel of Fig. 4, which shows the magnetically split line and a reference line observed in a non-magnetic star; a number of other spectral lines with more complex Zeeman patterns are also shown.

Let us denote the wavelength of the red spectral component of the split line by λ_r and its blue equivalent by λ_b. By Eq. 7, the shift of the red and blue components with respect to the undisturbed wavelength, λ_0, is given by

$$|\lambda_{b,r} - \lambda_0| = 4.67 \times 10^{-13}\ \text{Å}^{-2}\,\text{G}^{-1}\,\lambda_0^2 B |g_j m_j - g_i m_i| \quad (9)$$

$$= 4.67 \times 10^{-13}\ \text{Å}^{-2}\,\text{G}^{-1}\,\lambda_0^2 B \left|\pm\frac{1}{2} g_j\right| \ . \quad (10)$$

The last equation follows because one of the Landé factors (g_i) vanishes. Therefore, we obtain

$$\lambda_r - \lambda_b = 4.67 \times 10^{-13}\ \text{Å}^{-2}\,\text{G}^{-1}\,\lambda_0^2\,\langle B\rangle\,g_j \ , \quad (11)$$

where $\langle B\rangle$ is the "mean magnetic field modulus".

Exemplary estimation of magnetic field modulus: The separation of the components in Fig. 4 can be estimated to be roughly 0.3 Å. Substituting this into Eq. 11, we find a magnetic field modulus of $\langle B\rangle \approx 6$ kG. This is a strong fields compared to typical fields in sunspots, which are usually around 2 kG. Also note the essentially complete absence of any noticeable central (i.e., non-magnetic) line component, which indicates a high surface filling factor of the magnetic field.

It is clear that the above-demonstrated technique works best for strong, well-separated Zeeman components. This is the case, as long as the magnetic Zeeman splitting is strong compared to other sources of line broadening and the filling factors are large. Note that, e.g., sunspots typically cover less

than one percent of the solar surface. A particularly prominent source of non-magnetic line broadening is stellar rotation, but also contributions, e.g., by instrumental, thermal, or pressure broadening can be significant; especially in late-type stars also spectral line blends are a major nuisance. If other line broadening mechanisms dominate the magnetic splitting, the magnetic field provides yet another, often rather marginal, source of line broadening, which is challenging to detect. Observationally, the location of spectral lines is usually easier to determine than their width. To take advantage of this, another property of the Zeeman components is of paramount interest.

1.6 Polarization of the Zeeman components

Polarization describes the time dependence of the direction of the magnetic field vector of an electromagnetic wave.

1.6.1 The basics of polarization

The electric field vector of an electromagnetic wave traveling along the z-axis can be written as

$$\vec{E}(z,t) = E_x(z,t)\vec{e_x} + E_y(z,t)\vec{e_y} \ , \tag{12}$$

where

$$E_x(z,t) = E_{x0}\cos(\omega t - kz) \tag{13}$$
$$E_y(z,t) = E_{y0}\cos(\omega t - kz + \delta) \ . \tag{14}$$

For $\delta = 0$, the wave is linearly polarized, i.e., the direction of the electric field vector oscillates along a specific, time-independent direction. For $\delta = \pi/2$ and $E_{x0} = E_{y0}$, the wave is circularly polarized with the head of the electric field vector describing a circle when observed from the $\pm z$ direction. The sense of rotation of the field vector, as seen from an observer approached by the wave, defines whether the wave is right- or left-handed (clockwise or anticlockwise rotation). If neither of the above cases is realized, the wave is said to be elliptically polarized.

A popular way to parametrize polarization are the Stokes parameters I,Q,U, and V, which are usually summarized in the so-called Stokes vector. The Stokes parameters are the time-averaged values of specific combinations of the electric field component, in particular,

$$I = \langle E_x^2 + E_y^2 \rangle \tag{15}$$
$$Q = \langle E_x^2 - E_y^2 \rangle \tag{16}$$
$$U = \langle 2E_x E_y \cos(\delta) \rangle \tag{17}$$
$$V = \langle 2E_x E_y \sin(\delta) \rangle \ . \tag{18}$$

Here, I is the total intensity, Q and U describe linear polarization, and V describes circular polarization. For fully polarized light, the equality $I^2 = Q^2 + U^2 + V^2$ holds.

The Stokes parameters are measurable quantities. If, for instance, a beam of light can be split into its right- and left-handed circularly polarized components by an appropriate polarization filter and the resulting intensities I_R and I_L are measured, the Stokes V parameter can be computed as the difference between these intensities: $V = I_R - I_L$. Note that, therefore, the Stokes parameters Q, U, and V can be negative. Clearly, V is negative for left-handed circularly polarized light, positive for right-handed circularly polarized light, and zero for light without a preferred handedness. Also note that $I_L + I_R = I$.

1.6.2 Polarization of the Zeeman components

Depending on the orientation of the magnetic field, the Zeeman components show distinct polarization properties.

- *Transverse field*
  In this case, the π-components are linearly polarized parallel to the field. The σ-components are also linearly polarized, however, perpendicular to the magnetic field direction.

- *Longitudinal field*
  The π-components vanish and the σ-components are circularly polarized with opposite handedness.

1.6.3 Measurement of the longitudinal magnetic field

The polarization properties of the Zeeman components can be used to measure the longitudinal magnetic field. In particular, the idea is to measure the wavelength shift between the left- and right-handed circularly polarized light components, i.e., the σ-components. The concept is sketched in Fig. 5, where spectra obtained in Stokes I and V are sketched. Whereas the magnetic field produces a broadening of the spectral line in Stokes I, the individual circularly polarized components can still be separated. The central wavelengths of the $\sigma_\pm$-components shall be denoted by λ_R and λ_L.

Often, the Zeeman pattern is complex and consists of a number of $\sigma_\pm$-components (see, e.g., the lines shown in Fig. 4). If the individual spectral components cannot be resolved, $\lambda_{R,B}$ can be approximated by an intensity-weighted average of the individual σ-components. Let us assume a transition between two possibly magnetically split energy levels. The magnetic quantum numbers of the respective states shall be denoted by m_1 and m_2 and the respective relative strength of the components by $S(m_1, m_2)$. Further, $\Delta\lambda(m_1, m_2)$ is the wavelength shift of the component with respect to the undisturbed line. Then, the barycenter of $\lambda_{L,R}$ can be computed as (Mathys 1989, Eq. 2.39)

$$\Delta\lambda_{R,L} = \sum_{m_1,m_2;m_1-m_2=\pm1} S(m_1, m_2)\Delta\lambda(m_1, m_2) \; . \tag{19}$$

Here, $m_1 - m_2$ is restricted to either plus or minus one, depending on whether σ_+- or σ_- transitions (i.e., λ_R or λ_L) are under consideration.

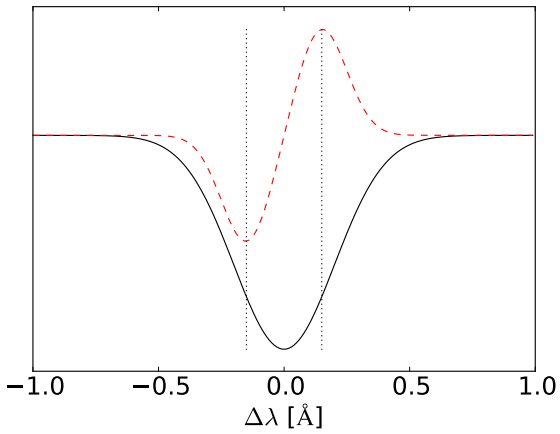

Figure 5: Sketch of magnetically split line observed in Stokes I (solid, black line) and Stokes V (dashed, red line). Dotted, vertical lines indicate the location of the $\sigma_\pm$-components.

The shift between λ_R and λ_L is often characterized by the "effective Landé factor", $\bar{g}$, so that

$$\langle\lambda_R\rangle - \langle\lambda_L\rangle = 2\bar{g}\Delta\lambda_z \langle B_z\rangle \quad \text{with} \quad \Delta\lambda_z = \frac{e\lambda_0^2}{4\pi m_e c^2} \; . \tag{20}$$

Here, $\langle B_z\rangle$ is the intensity-weighted longitudinal magnetic field. It can be shown that (e.g., Mathys 1989, Eq. 2.40)

$$\bar{g} = \frac{1}{2}(g_1 + g_2) + \frac{1}{4}(g_1 + g_2)[J_1(J_1 + 1) - J_2(J_2 + 1)] \; . \tag{21}$$

Figure 6 shows a spectral time series of Stokes I and Stokes V measurements presented by Mathys (1988) for the magnetic star HD 175362. The spectra are ordered by stellar rotation phase. The

Stokes V components shows a characteristic S-shape for some phases (cf., Fig. 5), while the profile is more complex for other rotation phases, indicative of more complex magnetic topologies.

Interpreting $\langle B_z \rangle$: The strength of the Zeeman components is not only a function of the magnetic field strength and orientation, but also of our viewing geometry, in particular, the angle, θ, at which we look onto the stellar atmosphere. This angle naturally varies between 0° at the center of the stellar disk and 90° at the limb; the angle is often expressed in terms of its cosine, in particular, $\mu = \cos(\theta)$, which is zero at the limb and one in the center of the disk. The behavior of the individual Zeeman components as a function of viewing angle is a problem of polarized radiative transfer, which shall not be discussed here; for an introduction see, e.g., Mathys (1989).

If $B_z(\nu, \phi)$ gives the strength of the longitudinal field component as a function of limb angle and azimuthal angle, ϕ, it can be shown that

$$\langle B_z \rangle = \frac{3}{2\pi} \int_0^{2\pi} \int_0^1 B_z(\mu, \phi) \mu^2 d\mu \; . \tag{22}$$

Note that a purely geometrically weighted average value would yield a factor of μ instead of μ^2 in the integration (plus a change in the preceding factors). The additional μ term is a result of radiative transfer (Mathys 1989, Eq. 4.11). Its presence puts a strong weight on the center of the disk where $\mu \approx 1$.

As a trivial and rather unphysical example, we may assume that $B_z(\mu, \phi) = B_{z,0}$, i.e., the longitudinal field component is identical across the entire disk. In this case we obtain

$$\langle B_z \rangle = \frac{3B_{z,0}}{2\pi} \int_0^{2\pi} \int_0^1 \mu^2 d\mu = B_{z,0} \; . \tag{23}$$

Not unexpectedly, the averaged value is identical $B_{z,0}$.

Alternatively, we may assume that the field is radial so that $B_z = B_0 \cos(\theta) = B_0 \mu$, which yields

$$\langle B_z \rangle = \frac{3}{2\pi} \int_0^{2\pi} \int_0^1 B_0 \mu^3 d\mu = \frac{3}{4} B_0 \; . \tag{24}$$

As another example, assume that there is a homogeneous longitudinal field around the center of the disk between $\mu = \mu_0$ and $\mu = 1$. With this assumption, we obtain

$$\langle B_z \rangle = \frac{3}{2\pi} \int_0^{2\pi} \int_{\mu_0}^1 B_0 \mu^2 d\mu = B_0 (1 - \mu_0^3) \; . \tag{25}$$

Of course we do not usually know the distribution of the field across the surface. Let us determine what fraction of the surface must be covered with the field so that we measure half the true (longitudinal) field strength. We have to determine a value μ_c so that

$$\frac{B_0 (1 - \mu_c^3)}{B_0} = 0.5 \quad \rightarrow \quad \mu_c = 0.8 \quad \rightarrow \quad \theta = 36^\circ \; . \tag{26}$$

This means that about one third of the visible stellar disk must be covered with the field, if it is distributed around the center of the disk—a result underlining that the central area of the disk is more heavily weighted in the average than its limb.

1.7 What can be learned from the observations?

The detection of non-vanishing longitudinal magnetic fields in Ap stars is indicative of large-scale field organization because the effect of oppositely directed small-scale longitudinal fields tends to cancel. This is also consistent with the absence of an "undisturbed" non-magnetic central component in the Stokes I profile of the Fe II λ6149.2 Å line, which shows a high magnetic filling factor.

The phase-dependent change in the spectral line profile seen, e.g., in HD 175362 and other magnetic Ap stars shows that the field cannot be rotationally symmetric around the stellar rotation axis. As

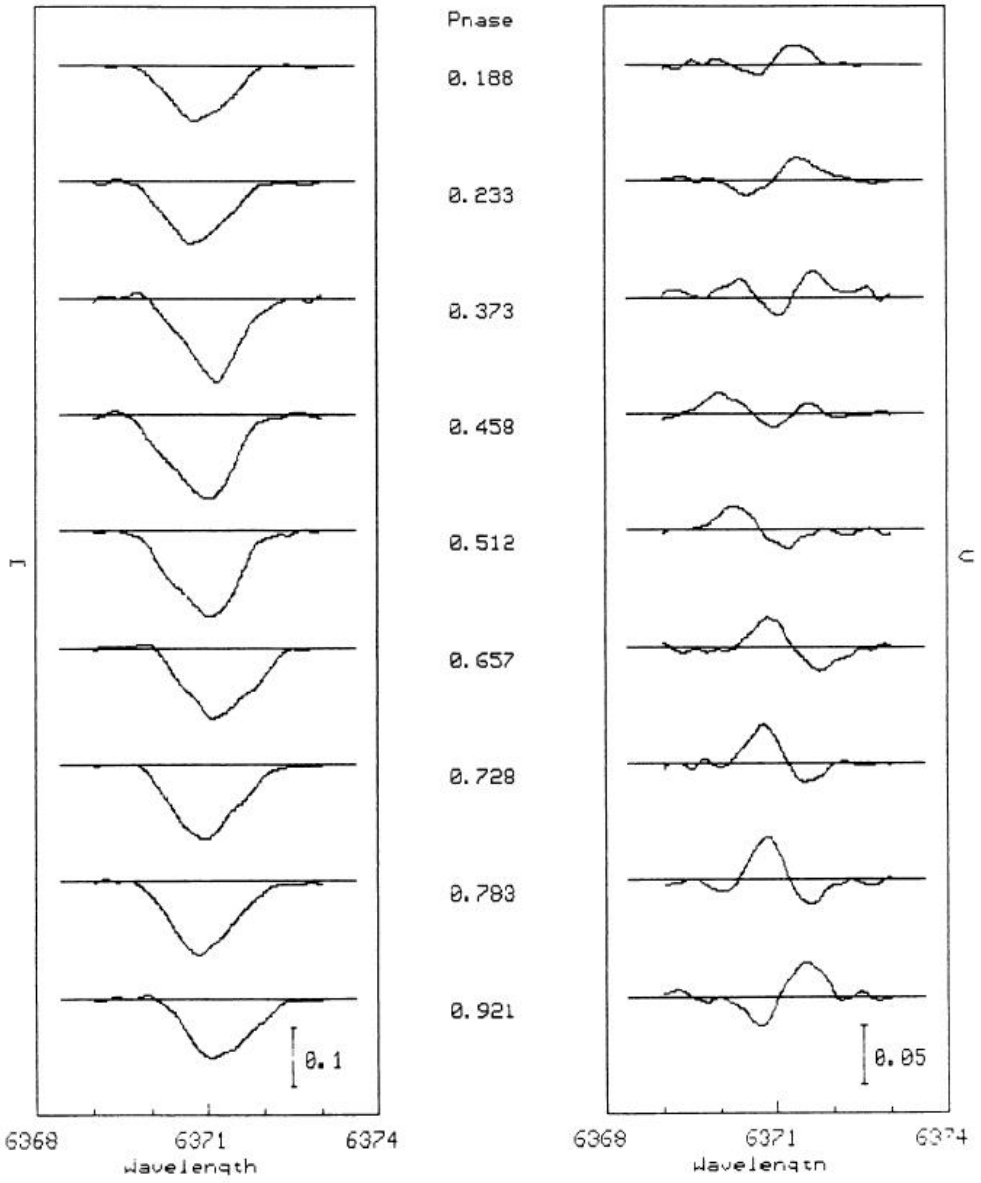

Figure 6: Spectral time series in Stokes I (left) and Stokes V (right) of the Si II line at 6371.3 Å of HD 175362. The spectra cover a rotational phase (from Mathys 1988, their Fig. 1). For some phases such as 0.657, Stokes V shows the characteristic S-shape, while the spectral profile is different in other phases, indicating more complex magnetic topologies.

one finds a relation between the projected stellar rotation velocity, $v \sin(i)$, and the "magnetic period", the variation is most likely due to stellar rotation (see, e.g., Landstreet 1992).

While it has not been explicitly be discussed here, it has been recognized that the longitudinal field does not tend to be significantly weaker than the mean magnetic field modulus. In fact, the observed value of $\max(< B_z > / < |B| >) \approx 0.3$ are consistent with a strong dipolar component of the field (Landstreet 1992).

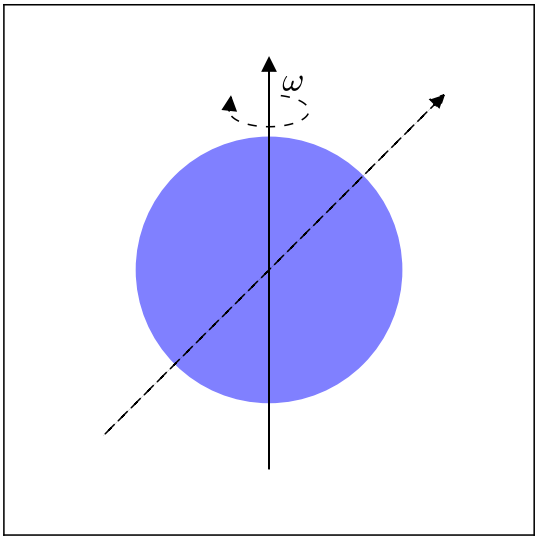

Figure 7: Sketch of the oblique (or rigid) rotator model. While the stellar rotation axis is vertical (solid arrow), the magnetic dipole axis is oblique (dashed arrow). This model provides large-scale field organization, a strong dipole component, and rotational asymmetry.

Taken together, these arguments suggest the oblique (or rigid) rotator model sketched in Fig. 7. Here, the star has a strong dipolar field component, which is however, tilted with respect to the stellar rotation axis. The viewing angle of the observer is, of course, arbitrary.

Clearly, the field of magnetic Ap stars is dramatically different from that of low-mass stars such as our Sun. The most widely accepted hypothesis for the origin of these large-scale magnetic fields asserts that they are essentially fossil, i.e., the fields are remnants of the field present in the medium from which the star formed. This hypothesis is, indeed, consistent with the observations of magnetic fields in stars with different ages and rotation rates, as well as estimates of the diffusion timescales (Landstreet 1992).

1.7.1 Magnetic fields and peculiar chemical abundances

It is thought that the existence of a strong magnetic field is also crucial in the formation of the observed chemical peculiarities. As it seems rather implausible that some ten percent of early-type stars are formed with dramatically non-cosmic elemental abundances, which are furthermore inhomogeneously distributed across the stellar surface, another mechanism has been developed to explain the observations.

The peculiar elemental (surface) abundances patterns can be explained in terms of diffusion processes, which have first been discussed in this context by Michaud (1970). The basic idea is that the magnetic field stabilizes the stellar atmosphere to a degree that allows diffusion processes to vertically separate the elements. In particular, the process is based on differential radiation pressure caused by the differences in the cross sections of the individual ions. This brings some elements to the top of

the atmosphere, while others settle down. The typical timescale for such a process to become relevant is 10^4 yr. Without the magnetic stabilization, disturbing processes such as mixing by differential rotation, overwhelm the effect of diffusion.

References

Hale, G. E. 1908, ApJ, 28, 315

Harvey, J. 1999, ApJ, 525, 60

Landstreet, J. D. 1992, A&A Rev., 4, 35

Mathys, G. 1988, A&A, 189, 179

Mathys, G. 1989, Fund. Cosmic Phys., 13, 143

Mathys, G., Hubrig, S., Landstreet, J. D., Lanz, T., & Manfroid, J. 1997, A&AS, 123

Michaud, G. 1970, ApJ, 160, 641